Silicon-rich SiO2/SiO2 multilayers: A promising material for the third generation of solar cell

F. Gourbilleau, C. Ternon, D. Maestre, Olivier Palais, C. Dufour

Silicon-rich SiO_2/SiO_2 multilayers: A promising material for the third generation of solar cell

F. Gourbilleau,[1,a)] C. Ternon,[1,b)] D. Maestre,[2] O. Palais,[2] and C. Dufour[1]
[1]*CIMAP, UMR CEA/CNRS/Ensicaen/Université de Caen, 6 Boulevard Maréchal Juin, 14050 Caen Cedex 4, France*
[2]*Université-Paul Cézanne-Aix-Marseille, IM2NP, UMR CNRS 6242, Av. Escadrille Normandie Niemen, 13397 Marseille-Cedex 20, France*

(Received 12 February 2009; accepted 23 May 2009; published online 1 July 2009)

Si-rich-SiO_2(SRSO)/SiO_2 multilayers (MLs) have been grown by reactive magnetron sputtering. The presence of silicon nanoclusters (Si-ncls) within the SRSO sublayer and annealing temperature influence optical absorption as well as photoluminescence. The optimized annealing temperature has been found to be 1100 °C, which allows the recovery of defects and thus enhances photoluminescence. Four MLs with Si-ncl size ranging from 1.5 to 8 nm have been annealed using the optimized conditions and then studied by transmission measurements. Optical absorption has been modeled so that a size effect in the linear absorption coefficient α (in cm^{-1}) has been evidenced and correlated with TEM observations. It is demonstrated that amorphous Si-ncl absorption is fourfold higher than that of crystalline Si-ncls. © *2009 American Institute of Physics*.
[DOI: 10.1063/1.3156730]

I. INTRODUCTION

Since the 1950s, with the publication of a new *p-n* junction photocell allowing the conversion of the solar radiation into electricity, solar-electric technology made huge progress in producing efficient converters.[1] The first goal was to increase solar cell efficiency, which was close to 5% in laboratory and 0.5% on commercial photocells during the 1950s. Besides, product development had to account for low cost and plentiful and nontoxic materials.

The first generation of solar cells was based on the use of mono- or polycrystalline silicon for which the main drawback concerns its indirect optical band gap requiring a thick active layer for the solar conversion and thus sophisticated and costly procedures to fabricate large area materials.

The aim of the second generation of photovoltaic (PV) material was to reduce the fabrication cost through the deposition of thin films allowing control over the quality of the material. Apart from the Si thin film fabrication, this led to the development of Cu-based ternary semiconductors such as $CdS/CuInSe_2$,[2–4] or $Cu(In,Ga)Se_2$.[5,6] Concerning Si-based and Cu ternary-based thin films, the literature reports conversion efficiencies in the 8%–26% range depending on the substrate and on the deposition process.[7]

The third generation of solar cells aims at increasing the efficiency of the PV conversion to decrease the cost per watt for producing future large scale devices.[8] Such an increase can be achieved by the use of multiple energy threshold devices such as the well known tandem solar cell, which is constituted of individual cells able to absorb different bands of the solar spectrum.[9] Thus, an all Si-based solar cell approach would require the fabrication of materials in which the Si band gap can be monitored. This has been possible since the 1990s with the discovery of the quantum confinement (QC) effect in porous silicon leading to an intense photoluminescence (PL) in the visible range at room temperature.[10] Such an emission has been deeply studied in $Si-SiO_2$ materials and ascribed to the confinement of the photogenerated carriers in Si grains whose size is smaller than 8 nm.[11–14] Besides the QC effect for explaining the new optical properties of nanometer-scaled Si films, some studies also pointed out the important role played by the Si/SiO_2 interface in the PL.[13,15–17] Thus, the PL of Si nanocluster (Si-ncl) is governed by key parameters such as grain size and the Si/SiO_2 phase separation. An efficient absorption of light by the solar cell can be reached through the optimization of the density of Si-ncl, the Si-ncl size for a control of the absorbed wavelength of the solar spectrum, and the Si/SiO_2 interface quality. Among all the fabrication techniques reported in the literature for providing photoluminescent Si-ncl, the most original ways to control the Si grain size are: (i) the laser pyrolisis of silane leading to the creation of free Si nanocrystals[18] or (ii) the deposition of Si/SiO_2 multilayers (MLs) in which the Si sublayer thickness should not exceed the critical value predicted by the QC model.[19–22] In addition to the control of the Si-ncl size, the ML approach offers the possibility to control the SiO_2 sublayer thickness, which is a key point for allowing the carrier transport through the multilayered structure.

In this paper, we describe the fabrication and the optimization of Si-rich silicon oxide (SRSO)/SiO_2 MLs using a reactive magnetron sputtering approach consisting in sputtering a pure silica target by hydrogen-rich plasma. We investigate the effects of the microstructure, the Si grain size and density, and the annealing treatment on the optical properties (infrared absorption, PL).

[a)]Electronic mail: fabrice.gourbilleau@ensicaen.fr.
[b)]Present address: Laboratoire des Technologies de la Microélectronique (LTM) Grenoble INP, CEA/LETI/D2NT, 17 Rue des Martyrs, 38 054 Grenoble Cedex 9, France.

II. EXPERIMENTAL

Thick SRSO/SiO_2 MLs have been fabricated by means of reactive magnetron sputtering. This process consists in sputtering a pure SiO_2 target with hydrogen-rich plasma for incorporating Si excess in the growing layer. Depending on the deposition parameters such as hydrogen partial pressure and substrate temperature, this process allows control of Si incorporation in the grown thin film as already reported.[17] For this paper, the MLs were deposited on quartz or (100) Si substrates maintained at 500 °C by an alternative reactive sputtering under hydrogen-rich plasma for growing the SRSO sublayer and under pure argon plasma to obtain the SiO_2 sublayer. The deposition time for these two sublayers allows control over their thickness and consequently the Si grain size within the SRSO sublayer. The power density applied for the sputtering of the SiO_2 target was 0.76 W cm^{-2}, whereas the hydrogen and argon partial pressures were fixed at 6.0 and 1.5 Pa, respectively. The microstructure of the MLs has been investigated through FTIR absorption spectra by means of a Nicolet 750-II spectrometer. The LO_3 and TO_3 vibrational modes of silica at about 1250 and 1080 cm^{-1}, respectively, are detected simultaneously by recording spectra at the Brewster angle of 65°. Energy filtered electron transmission microscopy (EFTEM) observations have been performed using a TEM JEOL-2010 F operating at 200 kV in the cross-section and plan view configurations allowing, for the former, to observe the stacking of each sublayer in the growth direction and, for the latter, to estimate the Si nanograins density. For this purpose, the samples in cross section have been thinned by means of a focused ion beam technique using Ga^+ ions to reduce the thickness of the samples down to 100 nm by an accurate control of the milling process. For the sample in the plan view configuration, a GATAN- precision ion polishing system has been also employed. The optical properties have been deduced from optical transmission measurements done in the 300–2500 nm range by means of a Perkin Elmer UV-visible spectrophotometer. Finally, the PL experiments allowing the control of the quality of the MLs were achieved using two different excitation lines, the 325 nm of HeCd laser and the 488 nm line of an Ar^+ laser.

III. RESULTS

A. Structure and emission properties of the (SRSO)/SiO_2 multilayers

A typical TEM image of a ML produced by means of this reactive approach is displayed in Fig. 1(a). This image clearly shows the perfect stacking of each sublayer having a thickness of about 3 nm. The sublayer presenting the darker contrast corresponds to the SRSO sublayer in which no Si nanocrystals can be detected as evidenced in Fig. 1(b). One can notice the presence of a thicker SiO_2 sublayer thickness (≈5 nm) in contact with the Si substrate due to the presence of SiO_2 natural native oxide on Si substrate.

The PL emission of an annealed ML under a 325 nm HeCd laser excitation is presented in the inset of Fig. 2 in the 600–1800 nm range. The higher noise in the 900–1800 nm range is due to the lesser sensitivity of the Ge detector with respect to the photomultiplier in the 550–900 nm range. One can notice the presence of a PL band peaking at about 800 nm in the visible region and two peaks (1100–1500 nm) in the IR one. The suitable deconvolution for such a spectrum is achieved considering two peaks (labeled *I* and *Q*) in the visible range, while four peaks (labeled E_1 to E_4) are necessary for the IR part as evidenced for the ML with the thinnest SRSO sublayer (1.2 nm) (Fig. 2). According to previous results reported in the literature,[23,17] the *I* and *Q* peaks are ascribed to the electron-hole recombination (i) at silicon/silica interface for the *I* peak and (ii) in the silicon nanograins within the frame of QC model for the case of the *Q* peak. A theoretical study[24] based on these experimental results has shown that both *I* and *Q* bands are superimposed on one another when some oxygen atoms are missing at the Si/SiO_2 interface saturated with Si=O double bonds. The E_1 to E_4 peaks are very close to those reported by Street in the

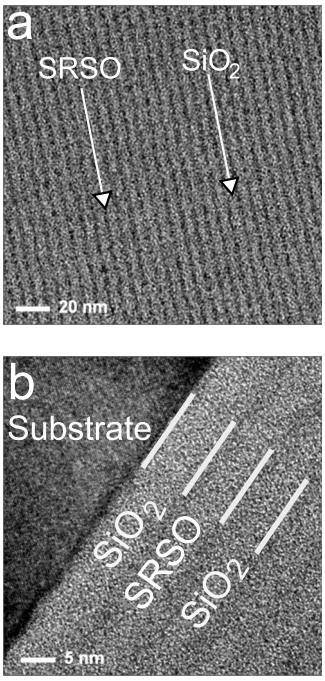

FIG. 1. Typical TEM images of a typical ML structure. (a) Bright field images showing the stacking of 3 nm thick SRSO and SiO_2 sublayers. (b) HREM images corresponding to the bright field observations in (a).

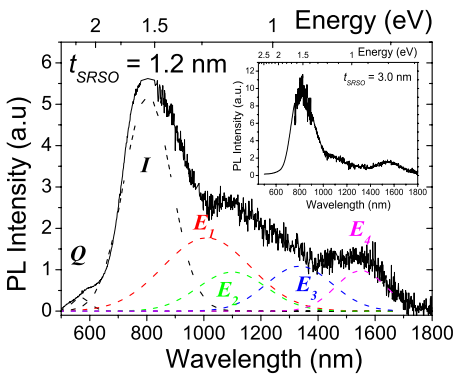

FIG. 2. (Color online) Typical PL spectrum recorded on a 1.2 nm-SRSO/3 nm-SiO_2 ML after an annealing at 1100 °C during 1 h. The inset shows the PL spectrum of a 3 nm-SRSO/3 nm-SiO_2 ML.

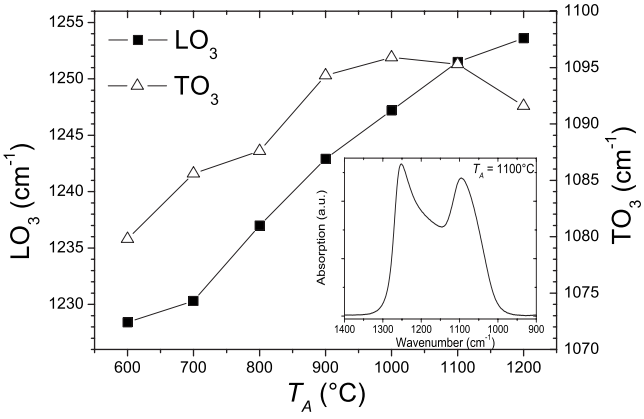

FIG. 3. Variation of the LO_3 (left scale) and TO_3 (right scale) phonon peaks for a 3 nm-SRSO/3 nm-SiO_2 ML as a function of the annealing temperature T_A. The inset shows a typical infrared spectrum for T_A=1100 °C.

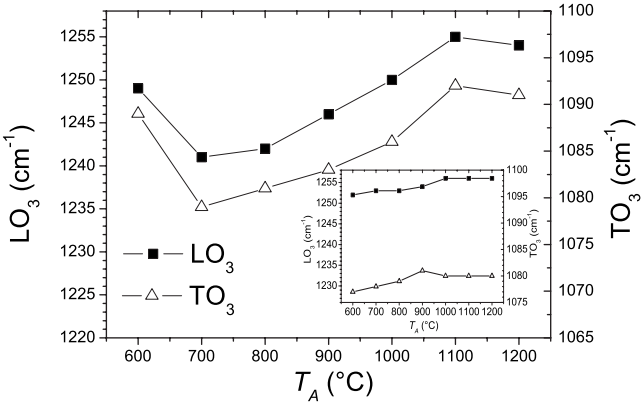

FIG. 4. Evolution of the LO_3 (left scale) and TO_3 (right scale) phonon peaks with annealing temperature T_A for a thick silica layer. The inset shows the corresponding ones recorded for a thick SRSO layer.

case of the amorphous silicon.[25] Consequently, their observation for both SRSO sublayer thicknesses can be explained by the presence of an amorphous Si phase in the SRSO sublayer even for t_{SRSO}=3 nm. This point is consistent with the work of Veprek *et al.*[26] who reported that the amorphous phase is more stable than the crystalline in Si grains whose size is smaller than 3 nm. More details on the dependence of the PL emission with t_{SRSO} and the corresponding modeling have been reported elsewhere.[17]

B. Annealing treatment

The effect of annealing temperature T_A on the 600–1100 °C temperature range has been studied on MLs having a 3 nm thick SRSO sublayer. FTIR absorption spectra (Fig. 3) show the evolution of the two main vibrational modes, LO_3 and TO_3, against the annealing temperature T_A, while the inset shows a typical FTIR spectrum recorded in the 900–1400 cm^{-1} range. The reported values evidence that the increase in annealing temperature leads to a shift of the LO_3 and TO_3 modes to higher frequencies, from 1225 to 1255 cm^{-1} and from 1075 to 1095 cm^{-1}, respectively. Since a ML is dealing with silica and SRSO sublayers, this evolution can be correlated with a structural rearrangement of silica or SRSO sublayers or both. To analyze the possible contribution of each sublayer, two reference samples consisting of a single thick silica or SRSO layers were fabricated and annealed at the same temperature than the ML. In order to be comparable with the studied ML, the thickness of each film was comparable to the total thickness of all the corresponding sublayers (silica or SRSO). The evolution of their LO_3 and TO_3 modes are plotted in Fig. 4 for the silica single layer and in the inset (Fig. 4) for the SRSO single film. The comparison of these two plots for either silica or SRSO thick layers to those of Fig. 3 for the MLs shows some similarities such as the steep increase in the frequencies of both the LO_3 and TO_3 modes of the ML (Fig. 3) and the concomitant shifts of these modes in the case of a single silica layer (Fig. 4), before becoming temperature independent for $T_A \geq 1100$ °C. Note that these modes are nearly unaffected by T_A for the single SRSO layer (inset of Fig. 4). Thus, one can assume that the evolution of the vibrational modes in the ML results from the progressive recovering of the silica defects with T_A, which seems complete after a treatment at 1100 °C.

HREM observations (Fig. 5) show the evolution of the ML microstructure as a function of the annealing temperature T_A. These observations have shown that a T_A as high as 900 °C is required to allow the formation of Si-ncls within the SRSO sublayer, which is in agreement with previous work.[20] The important role played by the interface in the control of the Si-ncl size is also evidenced since the average particle size of about 3 nm, which corresponds to the thickness of the SRSO sublayer, appears unaffected by the increase in T_A until 1100 °C. For T_A higher than 1100 °C, the Si grains grow beyond the SRSO/silica interfaces and reach a size of about 5 nm.

PL properties (Fig. 6) are presented as a function of T_A in the visible range of 400–850 nm, which corresponds to the optimal working range of the photomultiplier. For each spectrum, the corresponding fitting curves have been shown and the result of the accuracy of the fitting, R^2 added. Note that the intensity of these spectra does not present the same PL intensity depending on T_A and has been multiplied by the noted factor for allowing the PL comparison. These spectra show that the increasing T_A up to 1100 °C favors the PL emission increase in the ML, beyond this maximum annealing temperature, PL emission decreases. The result of the deconvolution for the ML annealed at 600 °C evidences the presence of three emission bands peaking at 450 nm (2.76

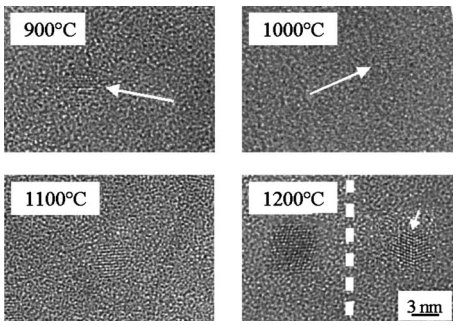

FIG. 5. HREM images of the MLs annealed from 900 to 1200 °C. For the highest temperature, the arrow indicates the presence of twin boundaries appearing within the nanocrystals.

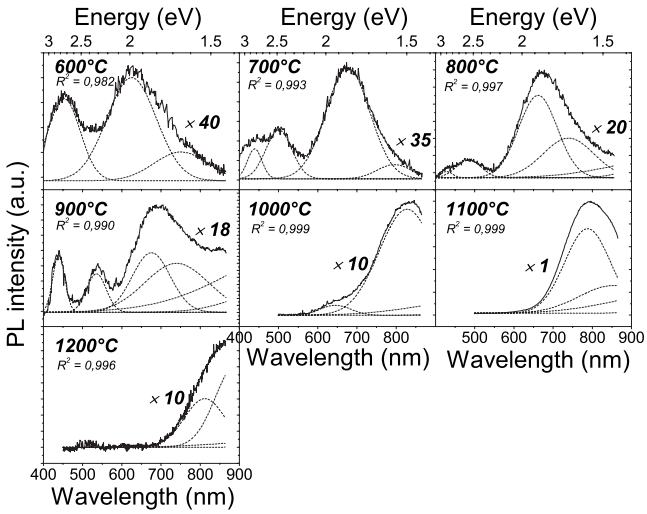

FIG. 6. PL spectra recorded in the 400–850 nm range of the 3 nm-SRSO/19 nm-SiO_2 MLs for the indicated T_A values. The scaling factors reported on the spectra are relative to the most intense spectrum recorded after an annealing treatment at 1100 °C.

eV), 625 nm (1.99 eV), and 750 nm (1.65 eV). When T_A is increased up to 700 °C, a fourth band appears at about 500 nm (2.48 eV), but for higher thermal treatment (>900 °C), two of these bands still remain clearly observable. The same measurements have been performed on the SiO_2 thick single layer (spectra not shown here). They show the presence of a weak emission at about 630 nm (2.0 eV) for the lowest T_A, which disappears when this layer is annealed at high temperature such as 1000 °C. The similarity with the ML PL behavior suggests that some of the bands observed with T_A can be related to the PL emission from optical transitions in the SiO_2 matrix, which are attributed to defects. These optical transitions correspond to three spectral regions: (i) from 1.85 eV (670 nm) to 2.0 eV (620 nm), (ii) at about 2.2 eV (564 nm), and (iii) from 2.4 eV (517 nm) to 2.8 eV (443 nm).[27–29] The peak positions of the emission bands obtained from the MLs (full symbols) and the silica layers (open symbols) have been plotted in Fig. 7 as a function of the annealing temperature, T_A. The above-mentioned three spectral regions are also indicated through the hatched areas. This graph shows that some of the PL emission bands recorded on our MLs when annealed at T_A<1100 °C can be related to the defects present in the silica host matrix, defects that are totally recovered for T_A=1100 °C as evidenced with the disappearance of these bands. Such notice confirms the deductions made on the evolution of the FTIR spectra described above. Concerning the related interfacial and QC bands, one can notice that both bands reach their maximum intensities in layers annealed at 1100 °C. The *Q* band is only affected by the annealing treatment with the occurrence of a shift toward the lower energy as well as a PL intensity decrease for the highest T_A imposed. This result is correlated with the Si grain growth and the formation of a nonrecombination site such as twin boundaries observed by HREM experiments (Fig. 5). Consequently, a thermal treatment at 1100 °C favors the optimum emission from Si nanocrystals and will be applied for the different MLs described hereafter.

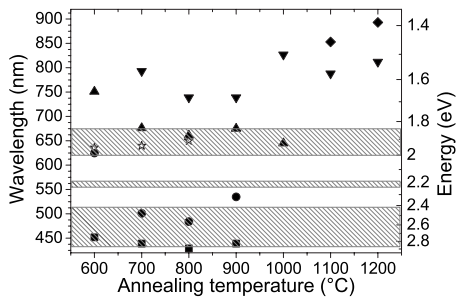

FIG. 7. PL peaks as a function of the annealing temperature T_A for the MLs (full symbols) and silica thick films (open stars). The hachured areas represent the emission range of silica defects.

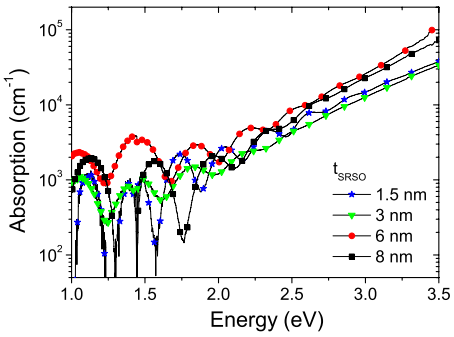

FIG. 8. (Color online) Absorption spectra of MLs for different SRSO sublayer thicknesses.

C. Absorption of the multilayers: Effect of the Si grains size and density

Four different MLs constituted by a 1.5 nm thick SiO_2 sublayer and a SRSO sublayer whose thickness t_{SRSO} varies from 1.5 to 8 nm have been deposited on fused quartz substrate. Depending on t_{SRSO}, the number of sublayers is ranging from 260, when t_{SRSO}=8 nm, to 704 for the thinnest SRSO sublayer in order to have a total film thickness of about 1.4 μm for all the layers. After the optimized annealing treatment at 1100 °C during 1 h as described above, these films have been studied by transmission experiments and the resulting linear absorption behavior with energy $\alpha_m(E)$ is reported on Fig. 8. Note that this coefficient has been determined by considering the total thickness of the SRSO sublayers for each ML. One can first notice the presence of oscillations on the spectra between 0.5 and 2 eV issued from reflections occurring between the film and the substrate. The analysis of the spectra evidences that the larger the grains, the higher the absorption in the whole range of energy. Considering a typical value of α_m of about 10^4 cm^{-1} at 2.5 eV for mono- or polycrystalline Si used for the second generation solar cells, the comparison with our data shows that the decrease in Si-ncl size seems rather having a detrimental effect on the absorption properties of the layer. To understand why such evolution is far from the one expected, microstructural investigations by means of plan view observations and EFTEM experiments have been performed on the MLs with SRSO sublayers 3 nm in thickness (Fig. 9). The plan view image evidences the presence of a high density of Si nanocrystals $\approx 10^{19}$ cm^{-3} whose size is 3 nm as shown in the bottom right part of the inset (Fig. 9).

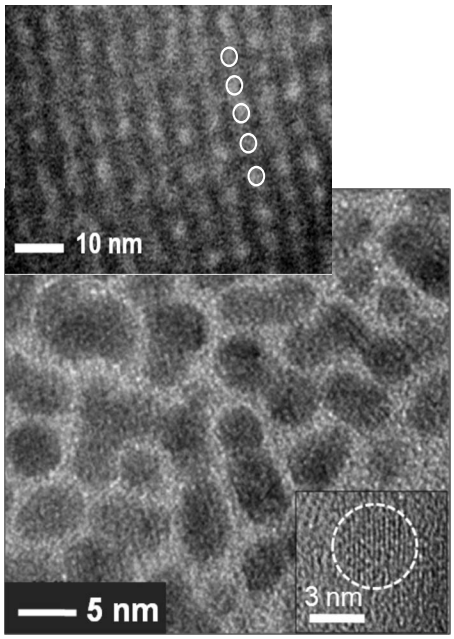

FIG. 9. Plan view image of the ML constituted of 300 alternations of 3 nm thick SRSO sublayers and 1.5 nm thick SiO_2 sublayers. The insets show a HREM image of a Si nanocrystals (bottom) and the cross sectional view of the ML by means of EFTEM (top).

The corresponding filtered image acquired on the cross sectional view using the 16 eV Si plasmon peak is displayed in the top left-hand inset of Fig. 9. This technique allows to evidence the presence of the Si-ncls whatever their orientation toward the electron beam. Thus, the embedded Si-ncls appear to be well distributed along the SRSO sublayer and are about 1.5 nm away from each other. Consequently, the value of the α coefficient determined above is not representative of the microstructure of the SRSO sublayer and a model taking into account the spherical shape of the Si-ncls as deduced from plan view and cross-sectional observations has been done and is described hereafter.

D. Absorption model

The following model aims at establishing a relationship between the measured absorption α_m in cm^{-1} and the absorption α_{grain} of silicon. We assume that the absorption of silica is negligible as compared to that of silicon. We base our study on the scheme shown in Fig. 10. The incident light

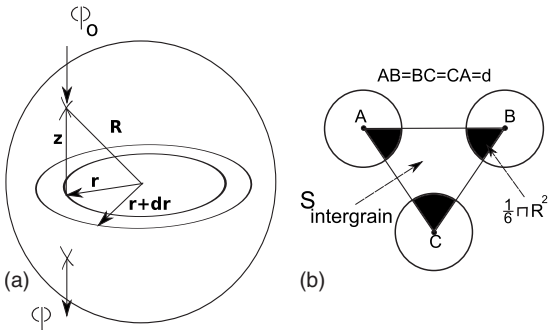

FIG. 10. (a) Scheme for modeling the corrected absorption. (b) Scheme for modeling the effect of the grain density: definition of the interfacial region.

TABLE I. Ratio α_m/α_{grain} between measured and pure bulk silicon absorption as a function of the grain radius R and the intergrain distance $d-2R$.

	R(nm)			
$d-2R$(nm)	0.75	1.5	3	4
0.5	0.34	0.44	0.51	0.535
0.8	0.257	0.377	0.47	0.5
1	0.217	0.34	0.44	0.477
1.5	0.15	0.268	0.386	0.427

strikes the sample under normal incidence with a given intensity I_0 with a uniform flux φ_0. Hence $I_0=\varphi_0 S_{ABC}$ where S_{ABC} is the sample surface [Fig. 10(b)]. We consider a part dI_0 of the light striking an elementary surface $dS=2\pi rdr$ located at a radius r from the center of the grain. At this point, a photon crosses a silicon thickness of $2z(r)$ so that the output flux dI is given by the Beer Lambert law, $dI=dI_0e^{-2\alpha_{grain}z(r)}=\varphi dS$.

Integrating this equation over all the surfaces (ABC), the transmission equation can be written as

$$\frac{I}{I_0}=\frac{1}{\pi R^2}\int_0^R e^{-2\alpha_{grain}z}2\pi rdr. \tag{1}$$

Accounting for $z^2+r^2=R^2$, the r into z variable change in Eq. (1) leads to

$$\frac{I}{I_0}=\frac{2}{R^2}\left[\left(-\frac{1}{2\alpha_{grain}}R-\frac{1}{4\alpha_{grain}^2}\right)e^{-2\alpha_{grain}R}+\frac{1}{4\alpha_{grain}^2}\right].$$

Now α_m and α_{grain} can be compared from a same measurement of I/I_0,

$$\frac{2}{R^2}\left[\left(-\frac{1}{2\alpha_{grain}}R-\frac{1}{4\alpha_{grain}^2}\right)e^{-2\alpha_{grain}R}+\frac{1}{4\alpha_{grain}^2}\right]=e^{-2\alpha_mR}. \tag{2}$$

We refine this model in order to account for the intergrain space [Fig. 10(b)]. Let d be the distance between two grain centers. The nonabsorbing surface between the grains is $S_{intergrain}=S_{ABC}-S_{grain}=(d^2\sqrt{3}/4)-\pi R^2/2$.

The measured transmission can be deduced as

$$\frac{I}{I_0}=\frac{\left[\int_0^R \varphi_0 e^{-2\alpha_{grain}z}\pi rdr\right]+\varphi_0 S_{intergrain}}{\varphi_0 S_{ABC}}. \tag{3}$$

Again we proceed to the same z into r variable change, we finally obtain

$$\frac{I}{I_0}=\frac{4\pi}{d^2\sqrt{3}}\left[\left(-\frac{1}{2\alpha_{grain}}R-\frac{1}{4\alpha_{grain}^2}\right)e^{-2\alpha_{grain}R}+\frac{1}{4\alpha_{grain}^2}\right]+1-\frac{\pi R^2/2}{\frac{d^2\sqrt{3}}{4}}. \tag{4}$$

The link between α_m and α_{grain} is established by comparing Eq. (4) and $e^{-2\alpha_mR}$. In Table I below, we report the ratio of the measured absorption (α_m) over the silicon absorption coefficient (α_{grain}) within the grains as a function of the grain

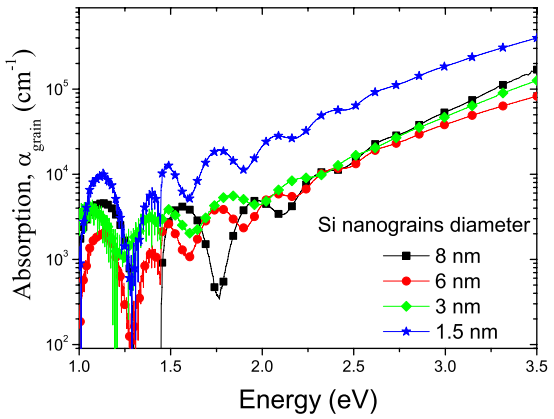

FIG. 11. (Color online) Absorption spectra of Si-ncls for different Si-ncl diameters ($2R$).

radius R_g and the intergrain mean distance d.

Thus, as expected, the absorption coefficient α_{grain} of the Si-ncl is always higher than the one (α_m) deduced from the transmission measurement. Taking into account the different nanograin radius of our MLs and fixing a mean distance d between nanograin of 1.5 nm as observed in the EFTEM images, the resulting evolution of α with the energy range for different Si grain diameter is reported in Fig. 11. The curves show that the lowest Si grain size offers the highest absorption coefficient, while for diameters in the 3–8 nm range, α is lower by a factor of 4 and the absorption curves almost similar. However, it has been previously demonstrated that the Si-ncls are amorphous below 3 nm.[17] Such a result means that the absorption coefficient α is higher in amorphous Si-ncl by a factor of 4 in comparison with its nanocrystalline counterpart. Consequently the use of Si-ncl as structure for absorbing the solar light should take into account this properties to optimize the yield of a future cell based on Si-ncls.

E. Electrical measurements

To demonstrate the potentiality of such a structure for wide band gap front cell of tandem solar cells, the electrical behavior of a SRSO/SiO_2 ML has been studied by means of two probe experiments under either darkness or UV illumination. For this purpose, a (3 nm-SRSO/3 nm-SiO_2 pattern) has been stacked 60 times on a p-type silicon substrate using the process described above before being submitted to an annealing treatment at 1100 °C during 1 h under pure nitrogen flux. Afterwards, Al dots of 1 mm in diameter have been deposited to create an Ohmic contact array with a step of 5 mm (Fig. 12). The I-V characteristics of the 360 nm thick layer have been recorded under darkness (cross) and UV illumination (stars) as reported in Fig. 13. The comparison between the two curves shows an increase in the conductivity of the device under UV illumination. To confirm the absence of any effect of the substrate in the conductivity process, I-V measurements have been performed under IR illumination (λ=940 nm are open circles in Fig. 13). The result reported in Fig. 13 shows that the behavior of the device is similar in darkness or under IR light, which demonstrates that the enhancement of the conductivity observed

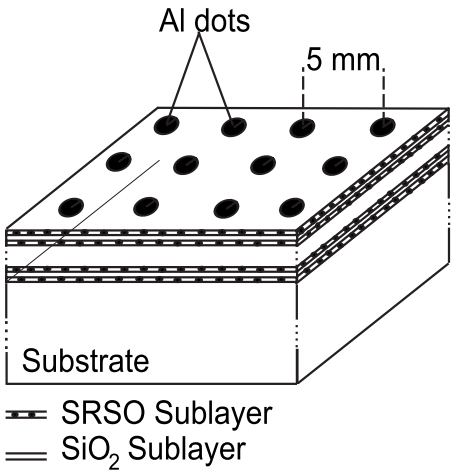

FIG. 12. Scheme of the device structure. The active layer is constituted of 60 [3 nm-SRSO/3 nm-SiO_2] patterns.

under UV illumination is attributed to a photoconductance effect of the nanostructured MLs. Moreover, it is worth noticing that the conductivity has been achieved in a "thick" mostly insulating layer and illustrates the interest of such a stacking structure in which the SiO_2 sublayer thickness and the Si nanograin density can be monitored.

IV. CONCLUSION

In this paper, we investigated the optical properties (absorption and PL) of Si-rich SiO_2/SiO_2 MLs fabricated using a reactive magnetron sputtering approach. The effect of the Si-ncl size, which can be easily controlled through the SRSO layer thickness, as well as the one of the annealing treatment, has been studied and analyzed. It appears that the optimized PL emission of the MLs has been obtained after an annealing as high as 1100 °C, whereas the presence of two peaks in the visible range has been observed in the PL spectra and is attributed to the interface and the QC effect in the Si-ncl. The resulting absorption coefficient has been determined for four different Si-ncl grain sizes after applying the optimized annealing treatment. The EFTEM-TEM observations allowed to evidence the microstructure of the MLs and more precisely the specific one of the SRSO sublayer. This has been helpful to evidence that both the Si-ncl size and density (cluster cm^{-2}) play a role on the absorption coefficient. The I-V measurements performed on a 3 nm-SRSO/3 nm-SiO_2

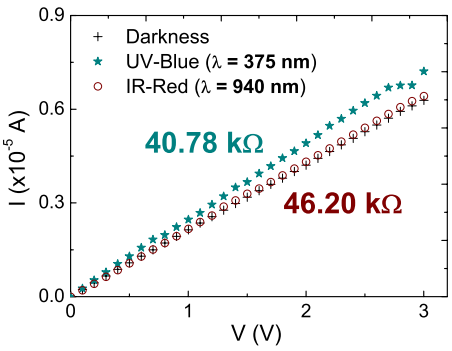

FIG. 13. (Color online) I-V measurements under darkness, IR, and UV illuminations.

ML demonstrate a photoconductance effect under UV illumination. The effect of the Si-ng size on the *I-V* characteristics are under progress before the realization and a test of *p-n* junction.

ACKNOWLEDGMENTS

Some of the authors want to thank Pr Xavier Portier for performing some of the HREM observations. This work has been supported by the ANR Solaire Photovoltaique through the DUOSIL project.

[1]D. M. Chapin, C. S. Fuller, and G. L. Pearson, J. Appl. Phys. **25**, 676 (1954).
[2]L. L. Kazmerski, M. S. Ayyagari, G. A. Sanborn, and F. R. White, J. Vac. Sci. Technol. **13**, 139 (1976).
[3]B. J. Brown and C. W. Bates, Jr., J. Appl. Phys. **68**, 2517 (1990).
[4]K. J. Hong, T. S. Jeong, and C. J. Youn, J. Appl. Phys. **100**, 123518 (2006).
[5]W. K. Metzger and M. Gloeckler, J. Appl. Phys. **98**, 063701 (2005).
[6]U. Malm and M. Edoff, Prog. Photovoltaics **16**, 113 (2008).
[7]L. L. Kazmerski, J. Electron Spectrosc. Relat. Phenom. **150**, 105 (2006).
[8]M. A. Green (unpublished).
[9]G. Conibeer, M. Green, R. Corkish, Y. Cho, E.-C. Cho, C.-W. Jiang, T. Fangsuwannarak, E. Pink, Y. Huang, T. Puzzer, T. Trupke, B. Richards, A. Shalav, and K.-L. Lin, Thin Solid Films **511–512**, 654 (2006).
[10]L. T. Canham, Appl. Phys. Lett. **57**, 1046 (1990).
[11]C. Delerue, G. Allan, and M. Lannooo, Phys. Rev. B **48**, 11024 (1993).
[12]N. A. Hill and K. B. Whaley, Phys. Rev. Lett. **75**, 1130 (1995).
[13]Y. Kanemitsu, Phys. Rev. B **53**, 13515 (1996).
[14]G. Allan, C. Delerue, and M. Lannoo, Phys. Rev. Lett. **76**, 2961 (1996).
[15]B. Garrido, M. Lopez, O. Gonzales, A. Perez-Rodriguez, J. R. Morante, and C. Bonafos, Appl. Phys. Lett. **77**, 3143 (2000).
[16]N. Daldosso, M. Luppi, S. Ossicini, E. Degoli, R. Magri, G. Dalba, P. Fornasini, R. Grisenti, F. Rocca, L. Pavesi, S. Bonelli, F. Priolo, C. Spinella, and F. Iacona, Phys. Rev. B **68**, 085327 (2003).
[17]C. Ternon, C. Dufour, F. Gourbilleau, and R. Rizk, Eur. Phys. J. B **41**, 325 (2004).
[18]G. Ledoux, O. Guillois, D. Porterat, C. Reynaud, F. Huisken, B. Kohn, and V. Paillard, Phys. Rev. B **62**, 15942 (2000).
[19]L. Tsybeskov, K. D. Hirshman, S. P. Dutlagupta, M. Zacharias, P. M. Fauchet, J. P. McCaffrey, and D. J. Lockwood, Appl. Phys. Lett. **72**, 43 (1998).
[20]M. Zacharias, J. Bläsing, P. Veit, L. Tsybeskov, K. Hirschman, and P. Fauchet, Appl. Phys. Lett. **74**, 2614 (1999).
[21]V. Vinciguerra, G. Franzò, F. Priolo, F. Iacona, and C. Spinella, J. Appl. Phys. **87**, 8165 (2000).
[22]F. Gourbilleau, X. Portier, C. Ternon, P. Voivenel, R. Madelon, and R. Rizk, Appl. Phys. Lett. **78**, 3058 (2001).
[23]Y. Kanemitsu and S. Okamoto, Phys. Rev. B **56**, R15561 (1997).
[24]E. Degoli and S. Ossicini, Surf. Sci. **470**, 32 (2000).
[25]R. A. Street, Adv. Phys. **25**, 397 (1976).
[26]S. Veprek, Z. Iqbal, and F. A. Sarott, Philos. Mag. B **45**, 137 (1982).
[27]R. Tohmon, Y. Shimogaichi, H. Mizuno, Y. Ohki, K. Nagasawa, and Y. Hama, Phys. Rev. Lett. **62**, 1388 (1989).
[28]S. Munekuni, T. Yamanaka, Y. Shimogaichi, R. Tohmon, Y. Ohki, K. Nagasawa, and Y. Hama, J. Appl. Phys. **68**, 1212 (1990).
[29]H. Nishikawa, E. Watanabe, D. Ito, and Y. Ohki, Phys. Rev. Lett. **72**, 2101 (1994).